QUIETDRONES 2024
MANCHESTER
8th - 11th September 2024

Acoustic Characterization of a Quadcopter Using a Test Stand

Session: Experimental Acoustic and Flow Measurements

Jared Schmal, University of Kentucky, USA, jared.schmal@uky.edu
D. W. Herrin, University of Kentucky, USA, david.herrin@uky.edu
Daniel Fernández Comesaña, Microflown Technologies, The Netherlands, fernandez@microflown.com

Abstract Unmanned aerial vehicles (UAVs) with multirotor propulsion and control, commonly referred to as drones, generate a complex acoustic field that is not entirely understood. Many components and their interactions contribute to the overall noise level and behavior of the acoustic field. A UAV test stand configured to emulate a small quadcopter was used to determine the acoustic response of a multicopter. A three-dimensional PU probe was utilized to obtain sound pressure, particle velocity, and sound intensity measurements close to the source, along with propagation planes for three-dimensional visualizations containing both amplitude and direction. Draw-away measurements using a PU probe were also completed to analyze the sound field characteristics further from the source. The number of propellers in operation was varied to determine the impact of adding additional sources. Aeroacoustic sources, near and far field behavior, interaction noise, directivity, and sound field propagation are discussed.

Keywords: Characterization; Directivity; Propagation; Interactions; Test Stand; Quadcopter

1. Introduction

Small unmanned aerial vehicles (UAVs) with multirotor propulsion and control, commonly referred to as drones, are becoming more prevalent in society. As of December 2022, over 1.47 million recreational UAV operators had registered with the US Federal Aviation Agency (FAA), with an estimated 1.69 million vehicles tied to these accounts [1]. While the growth rate in the recreational sector has waned in recent years, innovative commercial and military applications continue to persist. A prominent example can be seen in the Russo-Ukrainian War, where a dramatic shift in military tactics emerged. Thousands of drones are being used in all facets of the war along the front lines at any single moment [2]. Due to the recent number of drone-related attacks, Pentagon officials have decided to dramatically increase research and funding for counter-drone defenses [3]. Drones are also being utilized to replace conventional tasks in a more effective manner. For example, the rapid response time of drones has piqued the interest of first responders. In a trial performed in Sweden, drones successfully delivered defibrillators to victims of cardiac arrest, beating the ambulance to the scene 67% of the time [4]. Authorities are also utilizing drones for the surveillance of public spaces. In New York, drones are deployed to crime scenes as well as to detect sharks near public beaches [5], [6]. Hence, the presence of drones in our daily lives will become increasingly common as more industries explore the advantages of drone technology to improve their operations and services.

The utilization of drones will continue to grow as new and innovative uses are discovered, leading to the need for efficient acoustic testing on a wide range of drone types. However, difficulties arise in UAV measurements due to the complexity of replicating standard maneuvers in a controlled environment. Inherent risks to the vehicle, laboratory equipment, and technicians are present when a UAV is operated in an anechoic chamber. In addition, many standard acoustic measurements, such as sound intensity scans in the near field, are difficult to conduct due to the dynamic variability that occurs during flight. Therefore, a UAV test stand was designed to emulate a drone's behavior for rapid and safe acoustic measurements in a controlled environment.

Understanding the physical source mechanisms is a critical first step for prediction and detection models and design modifications for quieter operations. Therefore, the objective of this research was to utilize a test stand capable of replicating the acoustic behavior of drones for efficient measurement and analysis. Sound pressure and particle velocity measurements were completed to analyze a quadcopter's acoustic behavior, directivity, and decay rate in both near and far fields.

2. BACKGROUND

UAVs generate a complex acoustic field that is not entirely understood. Many components and their interactions contribute to the overall noise level and directionality of the acoustic field, but in most cases, the primary acoustic source is generated by the propellers [7]. Propeller noise can be decomposed into discrete components associated with tonal noise and continuous components related to broadband noise [8]. Tonal noise is produced by steady or unsteady periodic source mechanisms, while broadband noise is produced from unsteady random source mechanisms. The tonal response of a propeller mainly occurs at the blade pass frequency (BPF) and its harmonics, which are defined as

$$f_{\mathrm{BP}n} = \frac{nNR}{60} \;\; [Hz]\,, \tag{1}$$

where n is an integer, N is the number of blades, and R is the revolutions per minute of the motor shaft [9]. Propeller noise can be categorized into three primary sources: thickness noise, loading noise, and nonlinear noise [8]. Thickness and loading sources are relevant to UAVs, but nonlinear sources are only a factor for propellers approaching or exceeding supersonic speeds, and are therefore neglected in this analysis. Thickness noise is caused by the periodic displacement of flow over the blades and acts like a monopole source. Thickness noise is usually a discrete component, generating a tonal response that is primarily dependent on the propeller tip speed and becomes more significant as the propeller velocity increases. The airfoil shape, blade cord, and blade thickness are also variables related to thickness noise.

Loading noise can be steady and random, generating both tonal and broadband components, and can be modeled as a dipole source. The tonal component of loading noise is caused by periodic pressure fluctuations acting on the blade surface and are the same forces that generate lift and drag. Broadband loading noise is due to atmospheric turbulence or wake turbulence, caused by flow interactions from the airframe that are ingested back into the propeller stream. The airframe can be an important acoustic source due to interactions between the propeller and quadcopter arm, producing both tonal and broadband noise that is dependent on the receiver's location [10]. The phase of these sources can differ as well, leading to constructive and destructive interference, generating a highly directive and complex acoustic field [8].

The decay rate of a sound field can be useful for classifying acoustic sources. A monopole point source can be viewed as an omnidirectional pulsating sphere. The sound pressure of a monopole at position, $\mathbf{x}$, and at time, t, is defined as

$$p_{\text{monopole}}(\mathbf{x}, t) = \frac{\hat{Q}}{4\pi r} e^{\mathrm{i}\omega\left(t - \frac{r}{c}\right)}, \tag{2}$$

where $\hat{Q}$ is the source strength of a simple harmonic, r is the distance to the source, i is the imaginary number, ω is the angular frequency, and c is the speed of sound [11]. As indicated in Equation 2, the decay rate of a monopole for sound pressure is r^{-1}, regardless of the distance from the source. Therefore, the sound pressure of a monopole decays at a rate of 6 dB for each doubling of distance in the near and far field. However, the particle velocity of a monopole is more complex and contains two rates of decay. The particle velocity of a monopole is defined as

$$u_{\text{monopole}_r}(\mathbf{x}, t) = \frac{1}{\rho c}\left(1 + \frac{1}{\mathrm{i}kr}\right)\frac{\hat{Q}}{4\pi r} e^{\mathrm{i}\omega\left(t - \frac{r}{c}\right)}, \tag{3}$$

where ρ is the mean density and k is the wavenumber. The wave number can then be defined as

$$k = \frac{\omega}{c}. \tag{4}$$

In the near field, the particle velocity decays at r^{-2}, but transitions to decaying at the same rate as sound pressure in the far field. Hence, the particle velocity of a monopole decays at a rate of 12 dB in the near field and 6 dB in the far field, for each doubling of distance.

A dipole can be viewed as two closely spaced monopole sources of opposite phase. The sound pressure of a dipole is defined as

$$p_{\text{dipole}}(\mathbf{x}, t) = \frac{\mathrm{i}k\cos\theta}{4\pi r}\left(1 + \frac{1}{\mathrm{i}kr}\right)\hat{F} e^{\mathrm{i}\omega\left(t - \frac{r}{c}\right)}, \tag{5}$$

where $\hat{F}$ is the vector strength and θ is the angle between the dipole axis and the position, $\mathbf{x}$. Equation 5 indicates that the sound pressure of a dipole decays in the same respect as the particle velocity of a monopole source. The particle velocity of a dipole in the radial axis is defined as

$$u_{\text{dipole}_r}(\mathbf{x}, t) = \frac{\mathrm{i}k\cos\theta}{4\pi\rho c r}\left(1 + \frac{2}{\mathrm{i}kr} - \frac{2}{k^2 r^2}\right)\hat{F} e^{\mathrm{i}\omega\left(t - \frac{r}{c}\right)}. \tag{6}$$

In the near field, the particle velocity decays at two different rates, r^{-2} and r^{-3}, equating to 12 and 18 dB for each doubling of the distance from the source. The boundary between the near and far field can be difficult to define depending on the source, but generally, the near field can be defined as

$$kr \ll 1\,. \tag{7}$$

Therefore, the far field can then be estimated at values where $kr \geq 1$.

3. METHODOLOGY

A UAV test stand was configured to emulate a quadcopter with a wheelbase (diagonal length between each motor rotor) of 61 cm [12]. XRotor 40A electronic speed controllers (ESCs), T-Motor MN3508 brushless electric direct current (BLDC) motors, and 38.1 cm foldable carbon composite propellers were utilized. The stand was powered by two DC power supplies that simulate a six-cell battery pack with a nominal voltage of 22.2 V. A computer was used to send commands to an Arduino Mega 2560 microcontroller that allows each motor to be controlled and monitored independently. The Arduino sends pulse width modulation (PWM) signals to the ESCs as well as powers and records sensor information. The current input and the revolutions per minute (RPM) of each propeller were individually monitored using Hall effect and infrared (IR) sensor modules.

All measurements were conducted in the hemi-anechoic chamber located at the University of Kentucky. The chamber dimensions are 6.1 m × 6.1 m × 3.0 m and meets the ISO requirements for acoustic testing at 150 Hz and above. Hovering conditions were assessed, with each motor operating at approximately 3500 RPM, producing a stationary signal for the duration of the measurements. This allowed for scanning methods and frequency averaging to be used for spectral analysis. Two types of measurements were used to assess the acoustic behavior radiated from the UAV test stand.

3.1 Draw Away Measurements

Draw away measurements were completed to determine the directionality and decay rate. A Microflown PU probe was utilized to obtain both the sound pressure and particle velocity at the same point in space. Five propagation planes and six distances from the test stand were measured, doubling the distance from each point. The maximum distance that could be measured was limited by the dimensions of the anechoic chamber. Captures were recorded for thirty seconds and then averaged in the frequency domain. Two cases were analyzed as shown in Figures 1 and 2. A single propeller with the origin at the center of the propeller and a quadcopter configuration with the origin at the center of the test stand, equidistant from the blade tip of all four propellers.

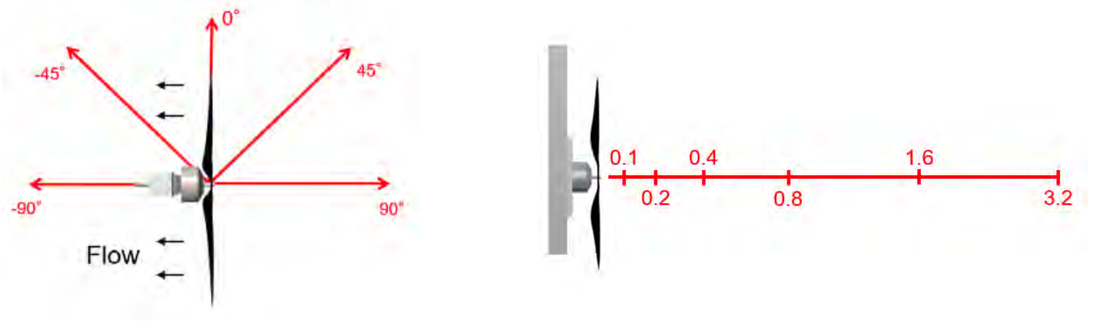

Figure 1: Draw away measurement locations using a single propeller (m).

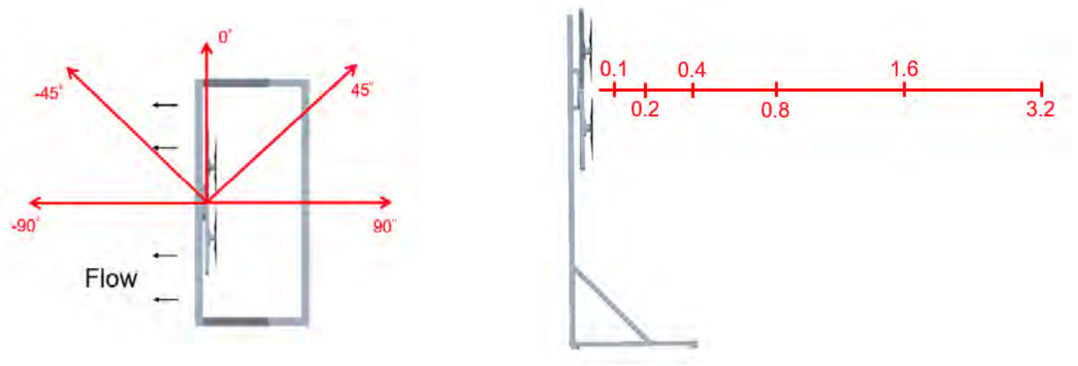

Figure 2: Draw away measurement locations using a quadcopter configuration (m).

3.2 Scan&Paint 3D

The Microflown Scan&Paint 3D solution is a portable measurement tool capable of visualizing an acoustic field in three dimensions [13]. The complete hardware list is detailed below and partially visualized in Figure 3.

Figure 3: Scan&Paint 3D measurement in operation (left) and enlarged 3D sound intensity probe (right).

- Microflown Voyager - A portable NVH analyzer and data acquisition system (DAQ)
- Laptop with Scan&Paint 3D software (Velo)
- PST Iris optical tracking camera
- Tracking sphere containing randomly spaced reflectors.
- Remote for single-user measurement control
- Microflown 3D sound intensity probe (Frequency range 20 Hz – 10 kHz)

The 3D sound intensity probe is manually moved along the measurement surface as the recorded signals and position are synchronized in real time. The sound field is then discretized into a cuboid grid over a 3D model of the object under test with a 1 cm cell resolution. The direction (sound intensity and particle velocity vectors) and magnitude of the sound field can then be calculated using the discretized sound pressure and orthogonal particle velocity signals [14]. For this research, the sound intensity probe was manually roved along the top and bottom propeller planes, approximately 5 cm from the propeller surface, to analyze the near field behavior. In addition, vertical propagation planes extending from the center of the test stand were captured at multiple angles. Two examples of captured measurement paths can be seen in Figure 4.

Figure 4: Sound intensity scanning paths: Top plane (left) and 90° propagation plane (right).

4. RESULTS AND DISCUSSION

The impact of flow-induced noise on the acoustic results was initially assessed due to the high-velocity airflow produced by the propellers. Figure 5 displays the spectrum for each measurement plane at a distance of 0.8 m from the propeller, representing the worst-case scenario. The flow is primarily generated directly beneath the propeller blades and only affects the acoustic results along the negative 90-degree plane. In this plane, flow noise is prominent at lower frequencies, decaying rapidly along the spectrum, and becomes negligible at approximately 450 Hz for both sound pressure and particle velocity. However, flow noise has a more significant impact on particle velocity, masking tonal components below 300 Hz, including the BPF. Please note that a standard foam wind cap was utilized. Better results can be achieved with a vendor-supplied wind cap specifically designed for particle velocity transducers.

Sound Pressure **Particle Velocity**

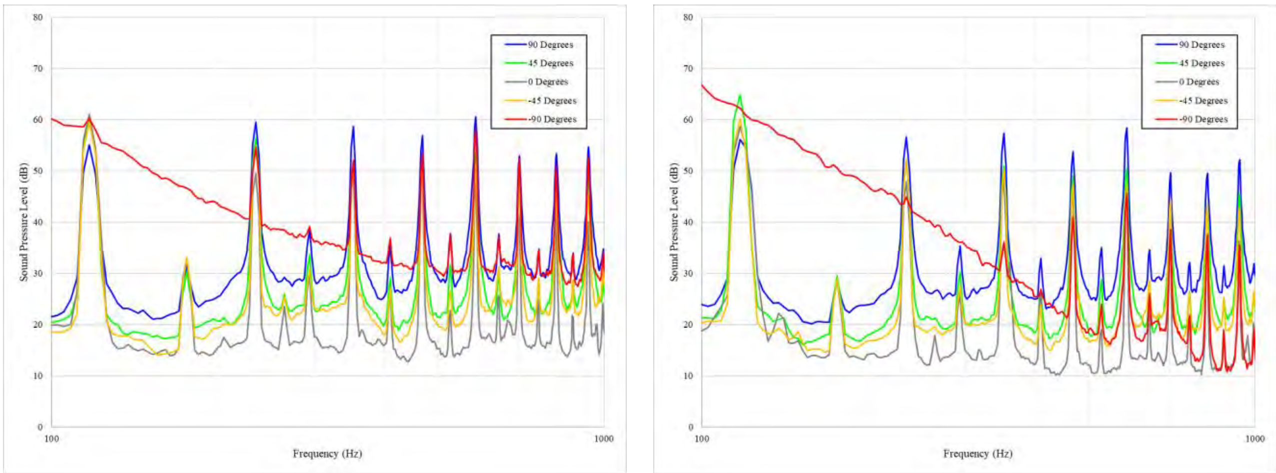

Figure 5: Sound pressure (left) and particle velocity (right) of a single propeller at 0.8 m from the source.

First, we discuss a single propeller case, which provides a simplified scenario for analyzing the propeller's acoustic behavior. An arm of the test stand was rotated vertically, and the motor mount was positioned towards the end of the arm to minimize interaction with the test stand frame. Figure 6 shows the near field A-weighted active sound intensity from 100 to 10,000 Hz for the top, propeller, and bottom planes after the volume around the operating propeller was scanned using the Microflown Scan&Paint 3D solution. The vector nature of sound intensity illustrates the propagation and magnitude of the acoustic field. The sound radiates perpendicular to the propeller axis, while rapidly dissipating in the propeller plane. Near-field acoustic behavior aligns with the propeller's rotational direction but transitions to propagate normal to the source with increased distance. The measurements of the top plane indicate a toroidal shape around the propeller's center, caused by the rotating dipole source around the propeller axis. It is likely that interference on the bottom plane is caused by turbulence from flow or arm interactions, which disrupt the typical dipole pattern.

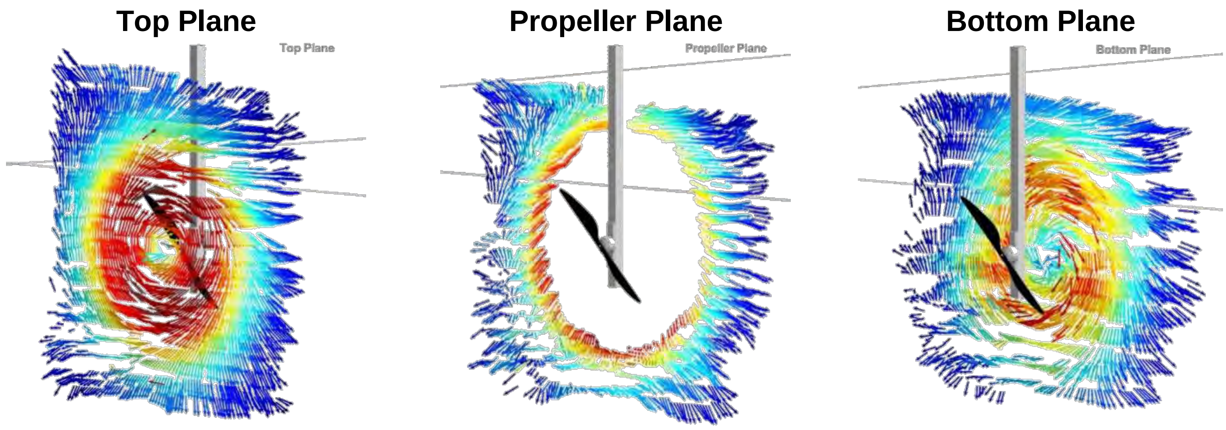

Figure 6: Broadband sound intensity of a single propeller on the test stand.

Figure 7 plots the sound pressure directivity of the BPF, 2nd, and 3rd harmonics for each distance from the source. Dipole behavior is evident in the near field but transitions to spherical propagation as the distance from the source increases. At 0.8m, the BPF loses symmetry due to flow noise, and directivity shifts to the underside of the propeller starting at 1.6m. The 3rd harmonic exhibits intriguing behavior at 0.2m, with acoustic energy dramatically shifting normal to the propeller plane.

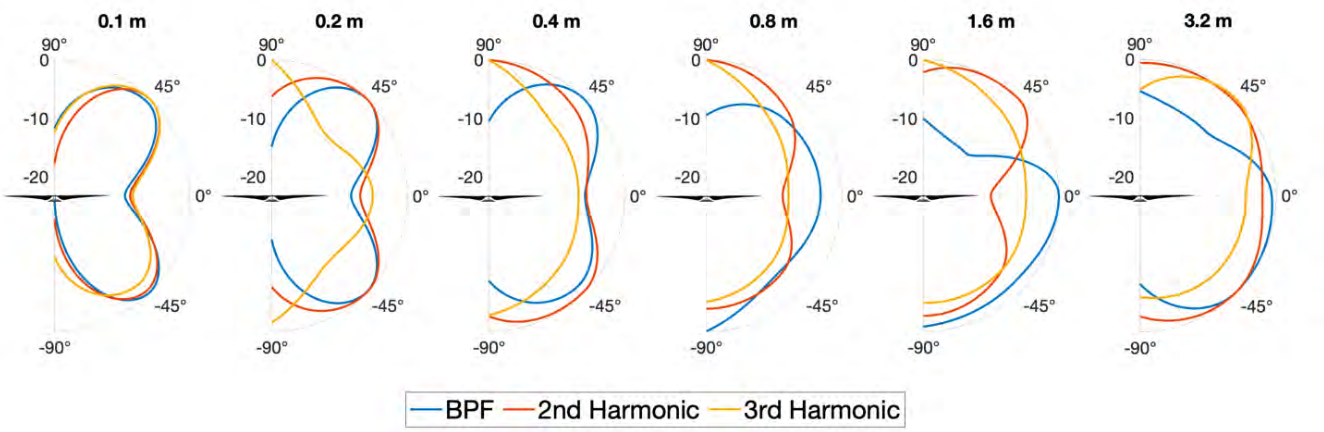

Figure 7: Propeller directivity of the BPF, 2nd, and 3rd harmonic of a single propeller as the distance from the source is increased.

Draw away measurements were used to calculate decay rates and are plotted against the wave number multiplied by the distance from the source (*kd*), enabling an analysis of the results in terms of acoustic wavelength. The measured vs theoretical decay rates of the BPF of a single propeller along the 90-degree plane are shown in Figure 8. Three decay rates can be observed with particle velocity (*left*) and two with sound pressure (*right*). This behavior is indicative of a dipole and implies loading noise to be the dominant acoustic source at the BPF. Velocity and pressure converge to approximately the same rate once the far-field is reached at *kd* equals 1.8, with the exception of an increase in sound pressure when kd equals 7.3. This increase is likely due to issues with approaching the edges of the anechoic chamber.

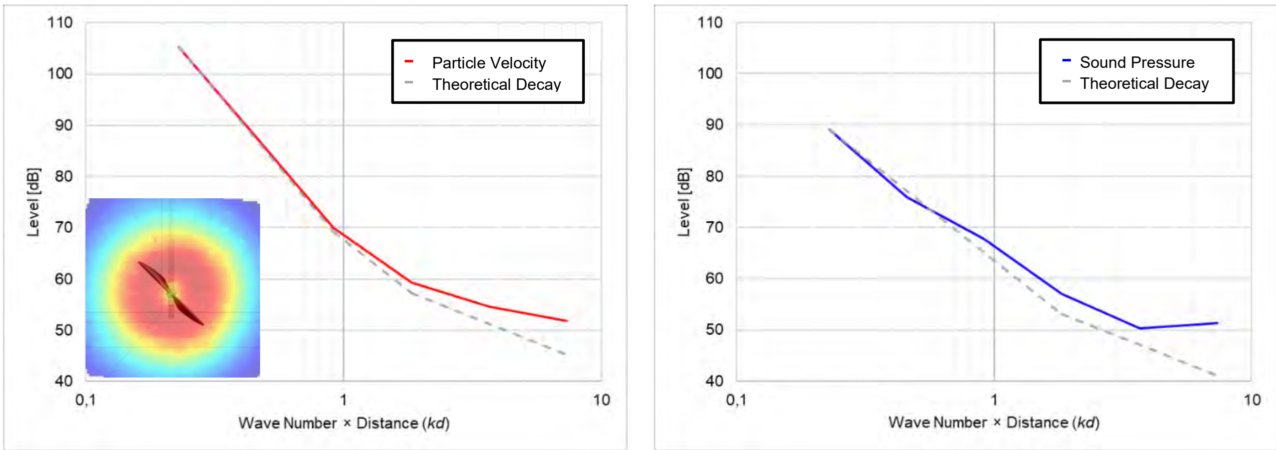

Figure 8: Measured vs theoretical decay rates of the BPF of a single propeller along the 90-degree plane.

Figure 9 shows the measured vs theoretical decay rates of the second harmonic of a single propeller along the 90-degree plane. Two decay rates are observed with particle velocity (*left*) and one with sound pressure (*right*). Hence, the second harmonic behaves like a monopole, indicating thickness noise as the dominant source.

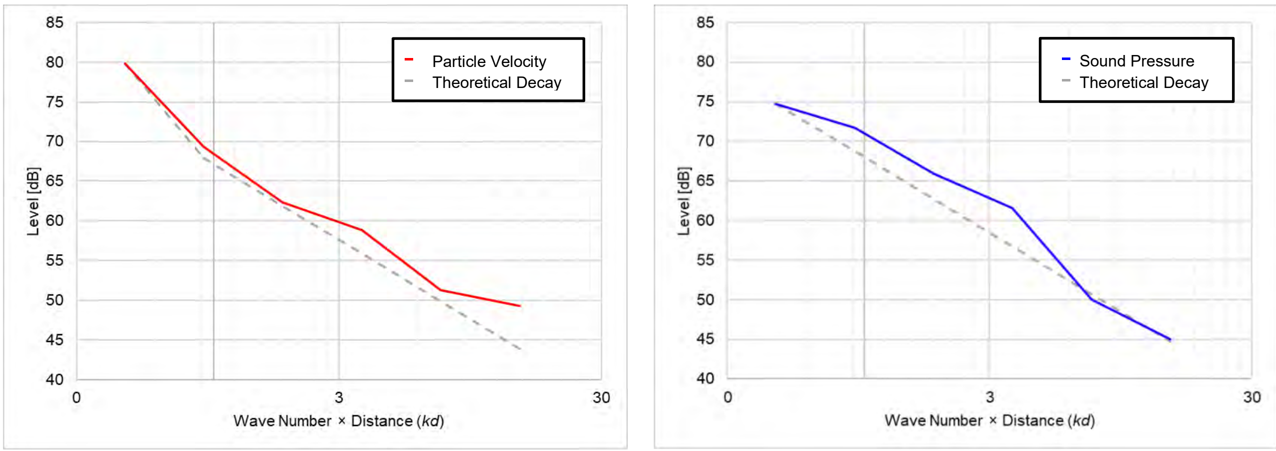

Figure 9: Measured vs theoretical decay rates of the 2nd harmonic of a single propeller along the 90-degree plane.

The sound pressure of the BPF and the second harmonic of a single propeller along the positive and negative 90-degree planes is shown in Figure 10.

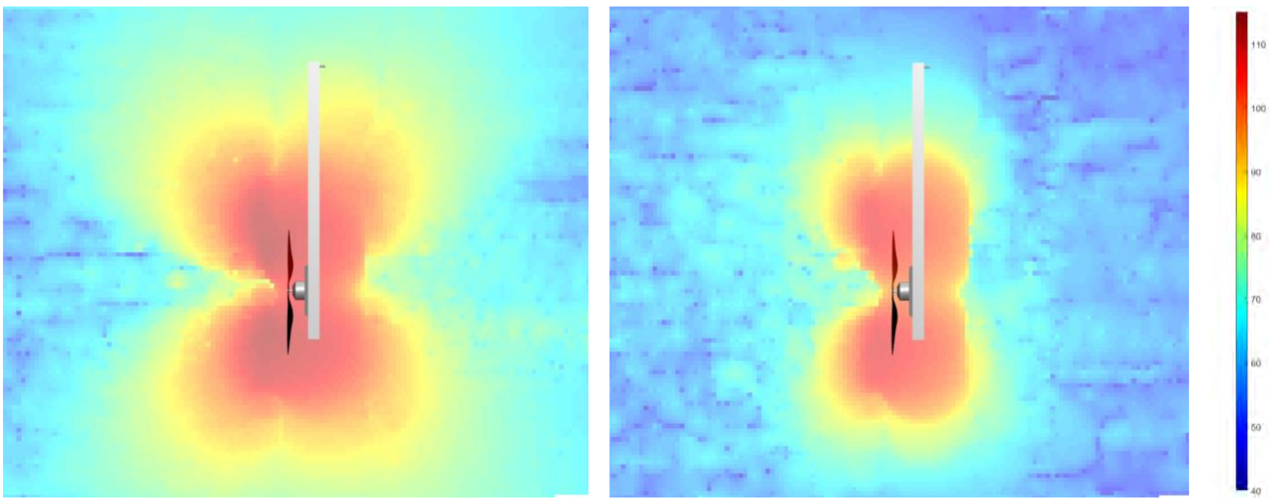

Figure 10: Sound pressure of the BPF (*left*) and 2nd harmonic (*right*) of a single propeller along the 90-degree planes.

Figure 11 visualizes the A-weighted active sound intensity of the BPF of a single propeller along the positive and negative 90-degree planes. Sound intensity's vector nature shows the propagation patterns and magnitudes of the acoustic field. At this low frequency, the dipole behavior is clearly visible. It is important to note that flow effects in the measurement can be seen in the bottom propagation plane.

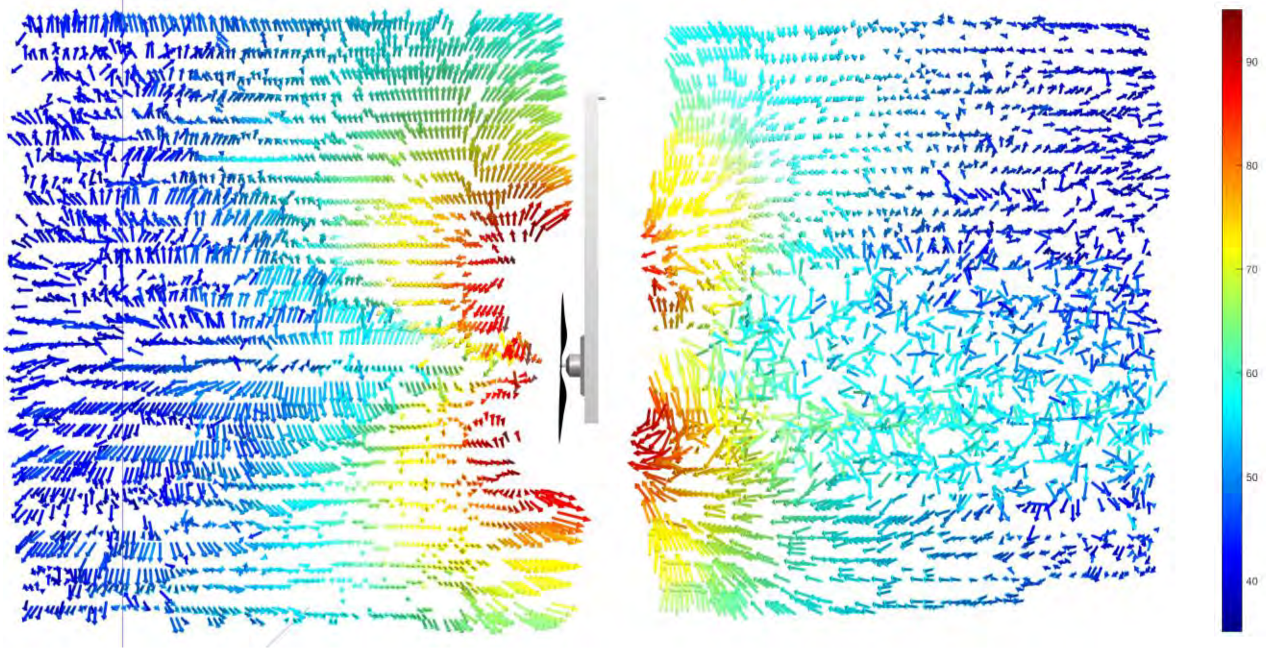

Figure 11: Active sound intensity of the BPF of a single propeller along the 90-degree planes.

Next, the quadcopter configuration was assessed to determine the acoustic behavior of the test stand while all four propellers were in operation. The near field A-weighted active sound intensity from 100 to 10,000 Hz for the top (*left*) and bottom (*right*) planes is shown in Figure 12. The direction of the sound intensity field over each propeller matches the rotation direction, and interactions are apparent at the blade tip boundaries. However, the acoustic behavior is clearly dominated by the propeller sources. Significant fragmentation can be visualized on the bottom plane due to turbulence flow and frame interactions.

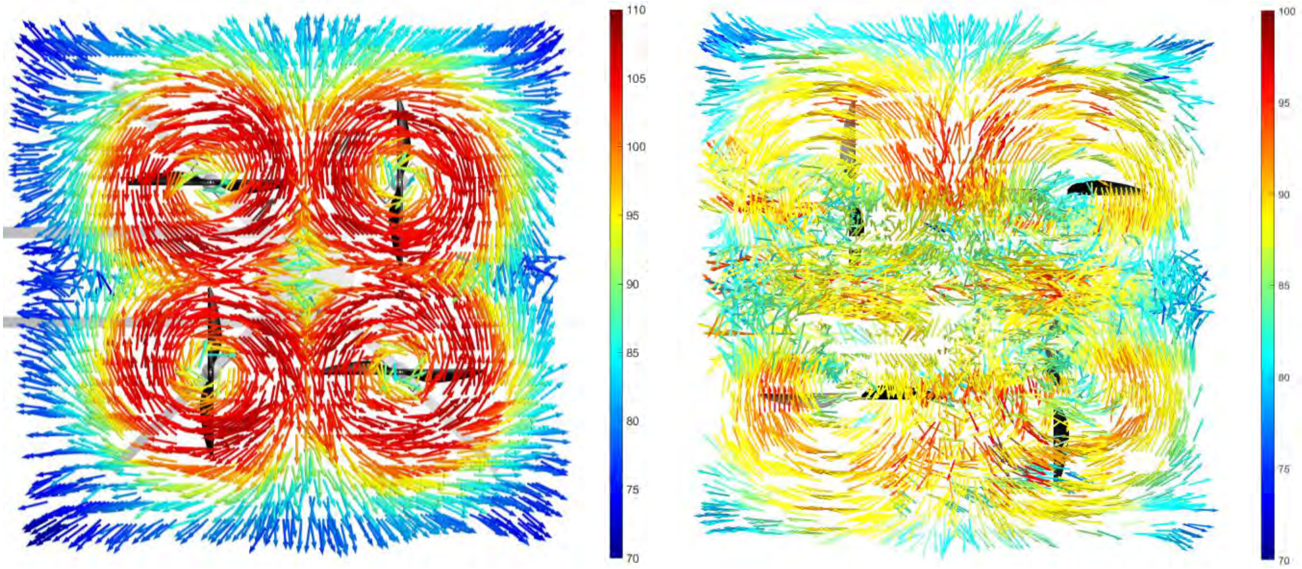

Figure 12: Near field broadband sound intensity of the quadcopter configuration. Top plane (*left*) and bottom plane (*right*).

Figure 13 is represented as a colormap in Figure 12 to enhance the visualization of the results.

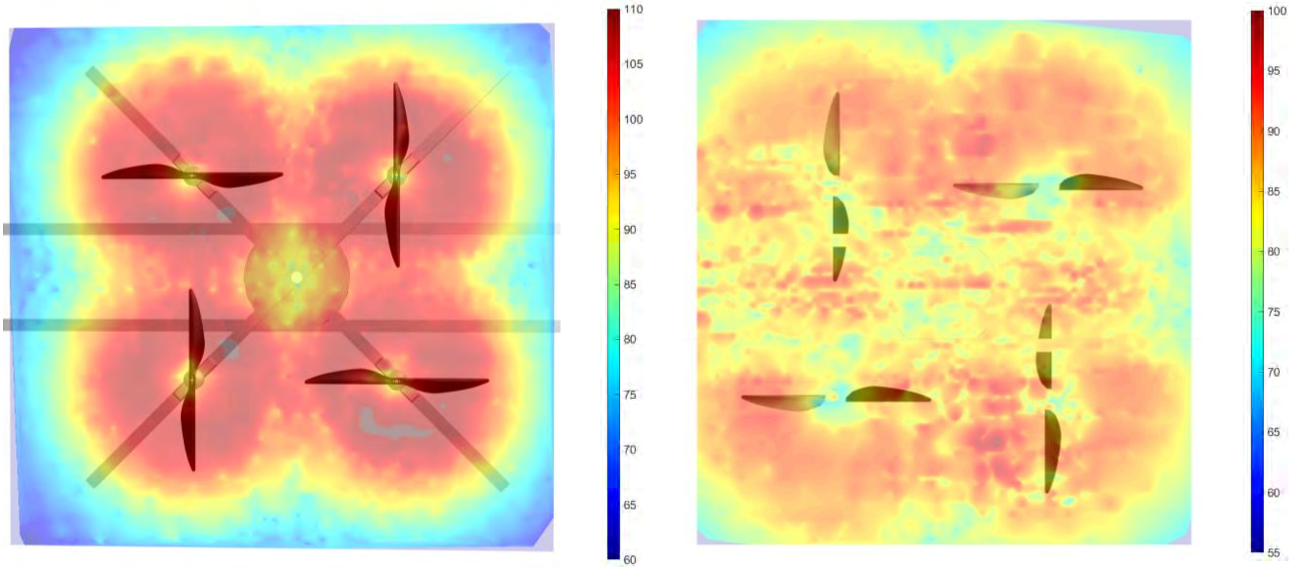

Figure 13: Near field broadband sound intensity of the quadcopter configuration. Top plane (*left*) and bottom plane (*right*).

Figure 14 plots the sound pressure directivity of the BPF, 2nd, and 3rd harmonics for each distance from the source when all four propellers are in operation. Similar behavior to the single propeller case is observed at the BPF, with dipole directivity in the near field transitioning to monopole directivity in the far field, and the majority of radiation shifting beneath the propeller at the furthest measurement point. However, unlike the single propeller case, the 2nd and 3rd harmonics largely maintain their dipole behavior in both the near and far fields.

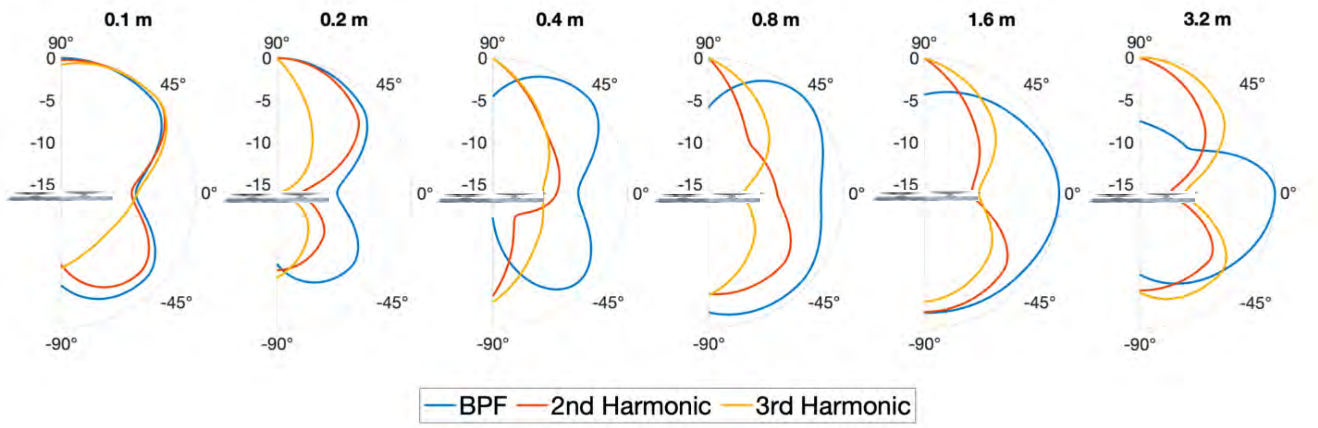

Figure 14: Propeller directivity of the BPF, 2nd, and 3rd harmonic of the quadcopter configuration as the distance from the source is increased.

Figure 15 shows the measured vs. theoretical decay rates of the BPF of the quadcopter configuration along the 90-degree plane. Three decay rates can be observed with particle velocity (*left*) and two with sound pressure (*right*). While more complex due to additional sources and the placement of the measurement probe, a similar scenario is shown compared to the single propeller case. Therefore, we can conclude this behavior is indicative of a dipole and implies loading noise to be the dominant acoustic source at the BPF. Velocity and pressure converge to approximately the same rate once the far-field is reached at *kd* equals 1.8.

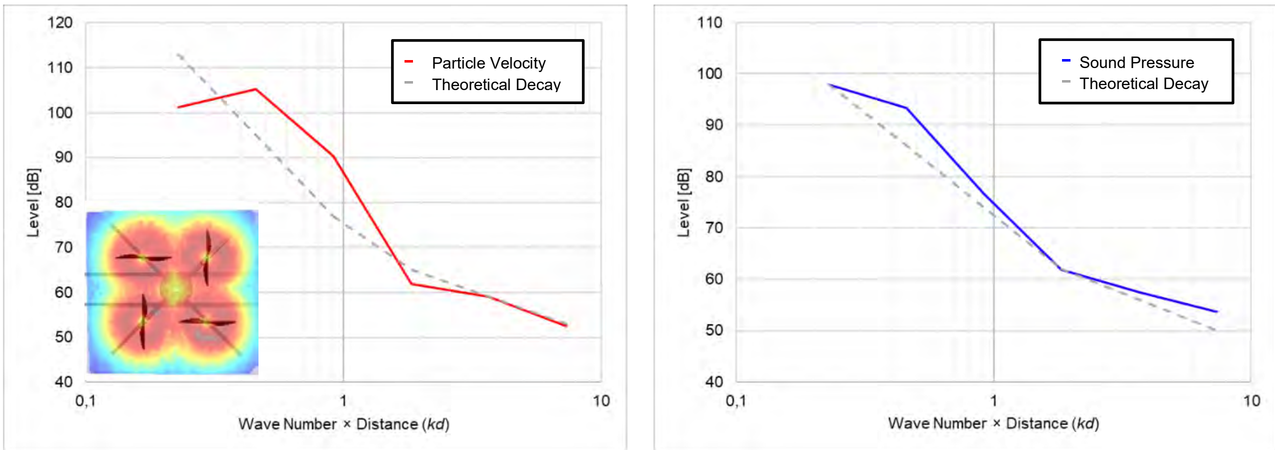

Figure 15: Measured vs theoretical decay rates of the BPF of a quadcopter (90-degree plane).

Figure 16 shows the measured vs theoretical decay rates of the 2nd harmonic of a quadcopter configuration along the 90-degree plane. As expected, two decay rates are observed with particle velocity (*left*) and one with sound pressure (*right*). As with the single propeller case, the second harmonic behaves like a monopole, indicating thickness noise as the dominant source.

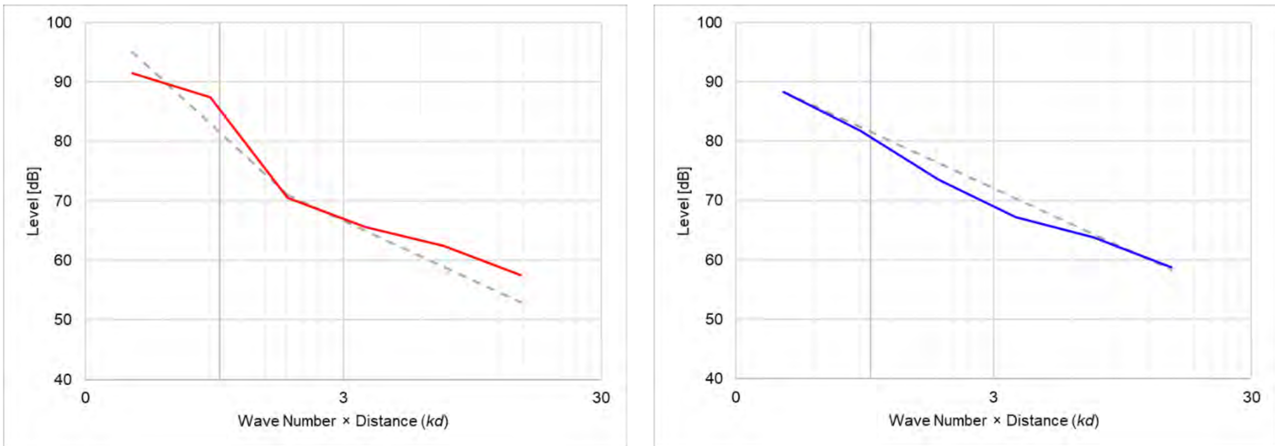

Figure 16: Measured vs theoretical decay rates of the 2nd harmonic of a quadcopter (90-degree plane).

The sound pressure of the BPF and the second harmonic of the quadcopter configuration along the positive and negative 90-degree planes is shown in Figure 17.

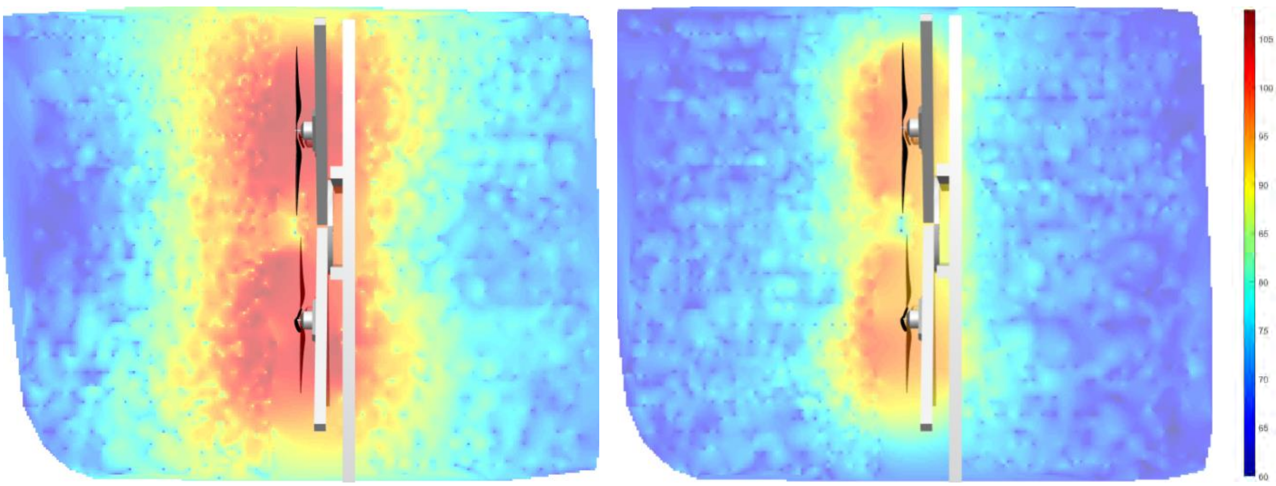

Figure 17: Sound pressure of the BPF (*left*) and 2nd harmonic (*right*) of a quadcopter configuration along the positive and negative 90-degree planes.

The complex acoustic behavior from the source interactions is notable. Figure 18 visualizes the A-weighted active sound intensity of the BPF of the quadcopter configuration along the positive and negative 90-degree planes.

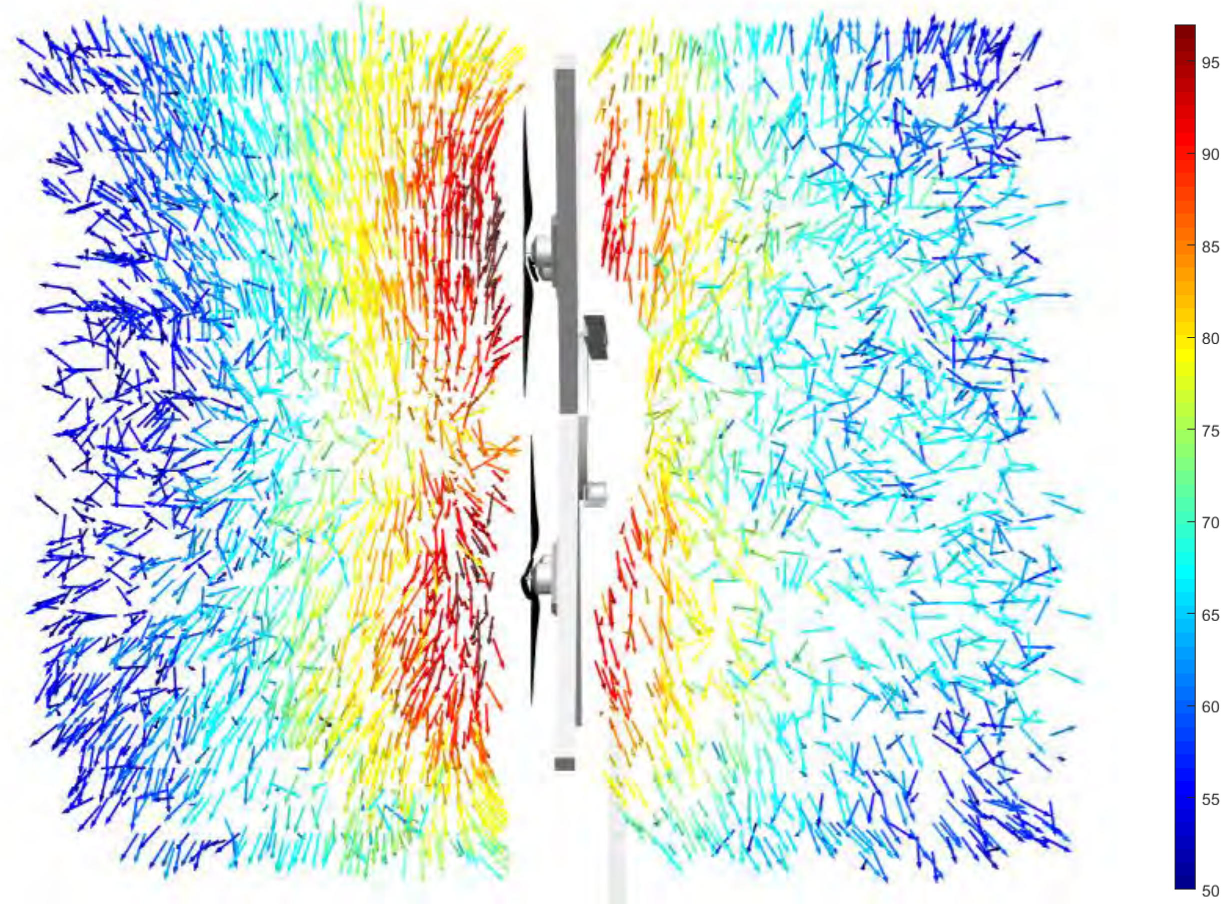

Figure 18: Sound intensity along a propagation plane perpendicular to the center of the test stand.

5. CONCLUSION

Sound intensity measurements were conducted on a UAV test stand, analyzing a single propeller and quadcopter configuration. Two types of measurements were performed: 3D sound intensity scans using Microflown Scan&Paint 3D and draw-away tests using a 2D sound intensity probe. All measurements were taken while the stand operated at approximately 3500 RPM, simulating a hovering quadcopter and producing a stationary sound field. The near-field behavior of the top (suction side) and bottom (flow side) of the UAV test stand was analyzed. Strong dipole patterns were observed on the top side of the quadcopter, while turbulence from flow effects and propeller-structure interactions likely caused fragmentation on the bottom side. The active sound intensity near the blades follows the rotational direction of the propeller and then transitions to propagate normal to the source. The draw-away measurements were utilized to determine the decay rate of sound pressure and particle velocity. In both the single propeller and quadcopter configuration cases, the BPF decay resembled that of a dipole, implying that loading noise is the primary acoustic source. Conversely, the second harmonic decay resembled that of a monopole, indicating that thickness noise is the dominant acoustic source. Sound intensity vectors and colormaps were then employed to effectively visualize this complex acoustic behavior along propagation planes perpendicular to the propeller surface.

ACKNOWLEDGMENTS

The authors gratefully acknowledge the support from the Vibro-Acoustics Consortium and Microflown Technologies.

REFERENCES

[1] M. Lukacs, "FAA Aerospace Forecast," Federal Aviation Administration, 2023.

[2] Y. Trofimov, "Drones Everywhere: How the Technological Revolution on Ukraine Battlefields Is Reshaping Modern Warfare," *The Wall Street Journal*, Sep. 28, 2023.

[3] D. Cameron, "Pentagon Eyes Microwave Weapons to Tackle Drone Threat," *The Wall Street Journal*, Dec. 19, 2023.

[4] S. Schierbeck *et al.*, "Drone Delivery of Automated External Defibrillators Compared with Ambulance Arrival in Real-life Suspected Out-of-hospital Cardiac Arrests: A Prospective Observational Study in Sweden," *Lancet Digit. Health*, vol. 5, no. 12, pp. e862–e871, Dec. 2023.

[5] B. Ostadan, "NYPD Chief Says Police Will Use More Drones at Crime Scenes," *Gothamist*, Aug. 27, 2023. [Online]. Available: https://gothamist.com/news/nypd-chief-says-police-will-use-more-drones-at-crime-scenes

[6] J. Gans, "New York to Deploy Shark-monitoring Drones to Beaches Following Reported Attacks," *The Hill*, Jul. 08, 2023. [Online]. Available: https://thehill.com/homenews/state-watch/4086719-new-york-to-deploy-shark-monitoring-drones-to-beaches-following-reported-attacks/

[7] N. Intaratep, W. N. Alexander, W. J. Devenport, S. M. Grace, and A. Dropkin, "Experimental Study of Quadcopter Acoustics and Performance at Static Thrust Conditions," in *The 22nd AIAA/CEAS Aeroacoustics Conference*, Lyon, France: American Institute of Aeronautics and Astronautics, 2016.

[8] M. J. Crocker, Ed., *Handbook of Noise and Vibration Control*. Hoboken, N.J: John Wiley, 2007.

[9] M. J. Crocker and J. P. Arenas, *Engineering Acoustics - Noise and Vibration Control*. Wiley, 2021.

[10] N. S. Zawodny and D. D. Boyd, "Investigation of Rotor–Airframe Interaction Noise Associated with Small-Scale Rotary-Wing Unmanned Aircraft Systems," *J. Am. Helicopter Soc.*, vol. 65, no. 1, pp. 1–17, 2020.

[11] M. J. Crocker, Ed., *Handbook of Acoustics*. New York: Wiley, 1998.

[12] J. Schmal, D. Herrin, and D. F. Comesaña, "Development of a UAV Test Stand," in *52nd International Congress and Exposition on Noise Control Engineering*, Japan, 2023.

[13] "Scan&Paint 3D | Visualizing 3D Sound Intensity," Microflown Technologies. [Online]. Available: https://www.microflown.com/products/sound-localization-systems/scan-paint-3d

[14] D. F. Comesanã, S. Steltenpool, M. Korbasiewicz, and E. Tijs, "Direct Acoustic Vector Field Mapping: New Scanning Tools for Measuring 3D Sound Intensity in 3D Space," presented at the EuroNoise, 2015.